CrystEngComm

Accepted Manuscript

ROYAL SOCIETY OF CHEMISTRY

www.rsc.org/crystengcomm

CrystEngComm RSCPublishing

ARTICLE

Structural and physicochemical aspects of hydrochlorothiazide co-crystals†

Cite this: DOI: 10.1039/x0xx00000x

Jian-Rong Wang,‡ Chanjuan Ye,‡ and Xuefeng Mei*

Received 00th January 2014,
Accepted 00th January 2014

DOI: 10.1039/x0xx00000x

www.rsc.org/

Crystal engineering principles were exercised in designing of new co-crystals of hydrochlorothiazide (HCT). A variety of potential co-crystal formers were initially identified in a search of the Cambridge Structural Database with complementary hydrogen-bonding functionalities. Subsequent co-crystallization screening monitored by powder X-ray diffraction led to the discovery of new crystalline phases of HCT with pyrazinamide (**1**), 4,4'-bipyridine (**2**), 1,2-bis(4-pyridyl)ethane (**3**), and *trans*-1,2-bis(4-pyridyl)ethylene (**4**). All the resulted co-crystals were thoroughly characterized by X-ray diffraction, FT-IR, Raman, and thermal analysis. Noticeably, the co-crystal **1** involves the formation of drug-drug co-crystal of HCT and pyrazinamide, which makes it a potential candidate for development of HCT formulations for combinational therapy.

Introduction

In many cases, undesirable biopharmaceutical characteristics rather than lack of efficacy or toxicity are more likely to hinder an active pharmaceutical ingredient (API) to be developed into a promising drug product.[1] Therefore, developing an appropriate solid form is of paramount importance for the success of a product. Different molecular arrangements within the solid may directly affect the physicochemical properties of the particular solid, such as hygroscopicity, stability, solubility, dissolution rate and bioavailability.[2] Currently, a variety of different solid forms, namely, amorphous, polymorphs, salts[3], hydrates[4], and solvates[5] have been called upon to alter the solid-state properties of a drug substance, particularly its solubility and bioavailability.[6] Due to the advent of supramolecular synthesis, co-crystals can be designed rationally utilizing the basic concepts of crystals engineering.[7] Therefore, for strategic co-crystal formation, it is critical to deeply understand the non-covalent contacts in the pharmaceutical co-crystals. The ease of preparation and the availability of various co-formers offer new opportunities for pharmaceutical co-crystals to have a broad prospect in becoming a solid form suitable for formulations in pharmaceutical development.

In order to go through efficient screening there must first be a design strategy. This has largely been focused on a synthon design approach[8] where a homosynthon has been disrupted in preference for a heterosynthon. Identifying reliable and robust supramolecular synthons is the key for effective crystal engineering. Cambridge Structural Database (CSD) provides valuable information on the occurrence of a particular supramolecular synthon in series of closely related structures, which may be applied to the synthesis of a wide range of co-crystals.[9] With over 700,000 small molecule crystal structures now available, we can harness structural knowledge more effectively than ever before in the context of co-crystal design and prediction. The design methodologies can now be performed using Motif Search technology in *Mercury*[10] or 3D searching in *ConQuest*[11].

Hydrochlorothiazide (HCT, Scheme 1) is a diuretic drug used for the treatment of hypertension and edemas. It belongs to a class IV compound according to the Biopharmaceutics Classification System (BCS), suffering from both low solubility (0.25 g/L) and low permeability (log P = -0.07).[12] The low bioavailability of HCT is partially attributed to its poor aqueous solubility. Attempts have been made by several groups in order to improve the solubility of HCT using various techniques. Captopril is used as a water soluble carrier and the solubility of HCT was enhanced from 0.25 mg/mL to 0.62 mg/mL when different concentrations of the carrier were applied.[13] Inclusion complex of HCT with β-cyclodextrin had also been synthesized to overcome the solubility limitations.[14] Co-crystallization approach was recently applied to HCT in order to alter its solubility. The synthesis and structure determination of co-crystals of HCT and isonicotinamide was reported by Zaworotko *et al.*[15] Co-crystals of HCT with nictinic acid, nicotinamide, succinamide, 4-aminobenzoic acid, resorcin, and pyrogallol have also been reported very recently.[16] The results have shown co-crystallization is a viable approach in improving HCT aqueous solubility.

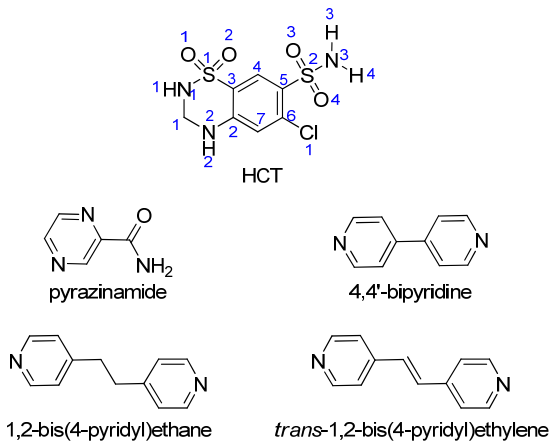

Scheme 1. Chemical structures for HCT and selected co-formers.

As the structure of HCT contains two sulfonamide and one aromatic amine groups, Scheme 1. Possible hydrogen bonding synthons are shown in Scheme 2. The CSD (version 5.35, February 2014) statistics (Table 1) reveal that aromatic nitrogen N_{arom} are dominant in forming H-bonding interactions with sulfonamide and amino groups (synthons **I** + **II**, 57%), followed by carboxylic acid (synthons **III** + **IV**, 36%) and amide (synthons **V** + **VI**, 4%). Analysis of the remaining sulfonamide or aromatic amide containing compounds reveals that they are involved in supramolecular synthons (3%) with different complementary functional groups such as phenol, ester, alcohol, etc. The above survey indicates synthons **I** and **II** are most frequent interactions expected in the co-crystal structure with HCT. Therefore, appropriate CCFs such as pyrazinoids and pyridinoids would be best suitable for co-crystallization design with HCT. A series of co-formers that may form synthons **I** or **II** were selected to co-crystallize with HCT, and four co-crystals of HCT with pyrazinamide (**1**), 4,4'-bipyridine (**2**), 1,2-bis(4-pyridyl)ethane (**3**), and *trans*-1,2-bis(4-pyridyl)ethylene (**4**) were successfully obtained.

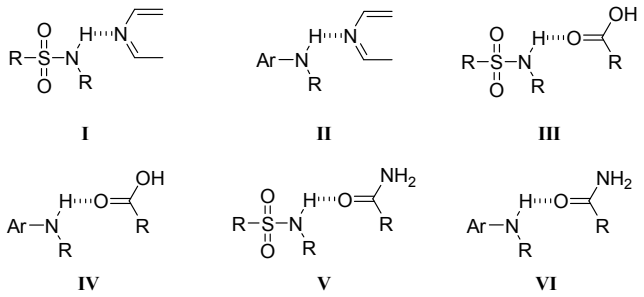

Scheme 2. Possible supramolecular heterosynthons for HCT with co-formers.

Table 1 CSD statistics of possible supramolecular synthons in HCT with different compounds

Compounds	Synthon	Hits	Total Hits with%
N_{arom}	**I** (Sulfonamide + Narom)	63	429 (57%)
	II (2° amine + Narom)	366	
Acid	**III** (Sulfonamide + acid)	64	273 (36%)
	IV (2° amine + acid)	209	
Amide	**V** (Sulfonamide + amide)	11	28 (4%)
	VI (2° amine + amide)	17	
Others	-	21	21 (3%)

Particularly, pyrazinamide is one of the most important front-line medicines for tuberculosis, and was found to be a suitable co-former with HCT. The co-crystal **1** is a drug-drug co-crystal which is classified as a subset of pharmaceutical co-crystals and can be used as candidates for development of combination drug products or fixed dose combinations.[17] While the electron-rich bipyridyl molecules, 4,4'-bipyridine, 1,2-bis(4-pyridyl)ethane, and *trans*-1,2-bis(4-pyridyl)ethylene, are frequently used as co-formers bearing good π-donors and hydrogen-bond acceptors. The structure aspects of the bipyridyl molecules introduces considerable flexibility and functionality in the construction of crystal lattice leading to variations in the networks thus formed. Many possible modes of association through strong and weak interactions make it interesting to explore the self-assembly of such system. The single crystal structures of **1**−**4** were solved and hydrogen bonding network, π-π stacking interaction were analyzed in detail. All the resulted co-crystals are thoroughly characterized by powder X-ray diffraction, FT-IR, Raman, and thermal analysis. The dissolution rate was compared between drug-drug co-crystal **1** and HCT itself.

Experimental

Materials

Hydrochlorothiazide (HCT), 1,2-bis(4-pyridyl)ethane and *trans*-1,2-bis(4-pyridyl)ethylene were purchased from J & K Scientific Limited. Pyrazinamide was purchased from Tokyo Chemical Industry Company Limited. 4,4'-bipyridine was purchased from Aladdin Chemistry Company Limited. All other chemicals utilized in this study were purchased as analytical grade.

Syntheses of 1−4

Co-crystals of HCT with pyrazinamide, 4,4'-bipyridine, 1,2-bis(4-pyridyl)ethane, and *trans*-1,2-bis(4-pyridyl)ethylene was synthesized by reaction crystallization method from ethyl acetate solvent. Firstly, into a 20 mL of ethyl acetate solvent, co-former powder (roughly 2.0 mmol) was suspended to give a saturated solution and the excess of solid was removed by

filtration. Then, an excess amount of HCT (0.3 mmol, 8.9 mg) was added to the saturated solution. The resulting suspension was allowed to react overnight at room temperature and subject for centrifugation to separate the solid phase. The co-crystal solid was harvested at the bottom of the centrifuge tubes, vacuum dried at 50 °C for 24 h to give corresponding co-crystals as fine crystalline powder.

For preparation of monocrystals suitable for single crystal X-ray diffraction analysis, the supernatant liquid of centrifugation was separated to concentrated at room temperature. Rod-shaped colorless single crystals were formed and the compositions of **1** (HCT / pyrazinamide, 1:1), **2** (HCT / 4,4'-bipyridine / H_2O, 2:3:2), **3** (HCT / 1,2-bis(4-pyridyl)ethane, 1:1), and **4** (HCT / *trans*-1,2-bis(4-pyridyl)ethylene, 1:2) were determined by single crystal X-ray diffraction.

Single crystal X-ray diffraction

X-ray diffractions of a single-crystal were performed on a Bruker Apex II CCD diffractometer using Mo Kα radiation (λ = 0.71073 Å) at 296 K. The structures were solved by direct methods and refined with full-matrix least-squares difference Fourier analysis using SHELX-97 software. Nonhydrogen atoms were refined with anisotropic displacement parameters, and all hydrogen atoms were placed in calculated positions and refined with a riding model. Data were corrected for the effects of absorption using SADABS. Crystallographic data in cif format have been deposited in the Cambridge Crystallographic Data Center, CCDC No. 989055-989058 for **1**−**4**, respectively. Crystallographic data and refinement details are summarized in Table 2.

.

Table 2 Crystallographic Data for co-crystals

Co-crystal	**1**	**2**	**3**	**4**
Formula	$C_{12}H_{13}ClN_6O_5S_2$	$C_{22}H_{22}ClN_6O_5S_2$	$C_{19}H_{20}ClN_5O_4S_2$	$C_{62}H_{64}Cl_2N_{14}O_8S_4$
Formula weight	420.87	550.05	481.99	1324.40
Crystal system	orthorhombic	monoclinic	monoclinic	monoclinic
Space group	$P2_12_12_1$	$P2_1$/n	$P2_1$/c	$P2_1$/c
Temperature (K)	296(2)	296(2)	296(2)	296(2)
a (Å)	7.673(6)	7.5201(11)	10.676(2)	11.2718(14)
b (Å)	13.318(11)	18.295(3)	23.734(5)	26.189(3)
c (Å)	16.250(14)	17.782(3)	8.5560(16)	21.160(3)
α (°)	90	90	90	90
β (°)	90	93.534(9)	95.786(8)	93.349(9)
γ (°)	90	90	90	90
Cell volume (Å3)	1661(2)	2441.7(6)	2156.9(7)	6235.8(14)
Calc. density (g/cm3)	1.683	1.491	1.478	1.411
Z	4	4	4	4
Independent reflections	2711	4291	3720	2672
S	1.022	0.939	1.017	1.022
R_1	0.054	0.048	0.067	0.091
R_{int}	0.079	0.159	0.085	0.092
w*R*	0.099	0.097	0.086	0.206

Powder X-ray diffraction

PXRD patterns were obtained using a Bruker D8 Advance X-ray diffractometer (Cu Kα radiation). The voltage and current applied were 40 kV and 40 mA, respectively. Samples were measured in reflection mode in the 2θ range 3−40 ° with a scan speed of 1.2 °/min (step size 0.025 °, step time 1.0 s) using a LynxEye detector. Data were imaged and integrated with RINT

Rapid, and the peaks are analyzed with Jade 6.0 software from Rigaku. Calibration of the instrument was performed using corindon (Bruker AXS Korundprobe) standard.

Fourier-transform Infrared (FTIR)

Fourier-transform Infrared (FTIR) spectra were collected by a Nicolet-Magna FT-IR 750 spectrometer in the range of 4000 to 350 cm^{-1} with a resolution of 4 cm^{-1} at ambient conditions.

Raman Spectroscopy

Raman spectra were recorded with a XPH-300 hot stage attached to the Thermo Scientific DXR Raman microscope equipped with a 532 nm laser. Raman scans range from 3500 to 50 cm^{-1}. Samples were analyzed directly in a glass sheet using 10 mW laser power and 50 μm pinhole spectrograph aperture. Calibration of the instrument was performed using polystyrene film standard.

Thermogravimetric Analysis (TGA)

Thermogravimetric analysis was carried out on Netzsch TG 209 F3 equipment with a typical scan range of 30−400 °C, scan rate of 10 °C/min and a nitrogen gas flow of 20 mL/min.

Differential scanning calorimetry (DSC)

Differential scanning calorimetry (DSC) was conducted in T zero aluminum pans using a TA Instruments Q2000 unit under nitrogen gas flow of 20 mL/min purge. Samples weighting 3−5 mg were heated in standard aluminum pans at scan rates from 5 to 10 °C/min. Two-point calibration using indium and tin was carried out to check the temperature axis and heat flow of the equipment.

Solubility and dissolution

HCT was slurred overnight in ethyl acetate at room temperature, the same process as that for co-crystallization of **1**−**4**. Dissolution tests of all sample crystals of HCT and co-crystals **1**−**4** were carried out on the 250−350 μm sieve fraction cut to minimize the size difference effect.[18] HCT concentration of the solutions in dissolution and solubility experiments was determined by USP HPLC assay method. The HPLC instrument (Agilent 1260 series)was equipped with an Agilent Eclipse plus C18 column (4.6 mm × 150 mm × 3.5 μm). The detection wavelength was set at 275 nm with injection volumn of 10 μL and the eluent flow rate of 1 mL/min. The mobile phase is acetonitrile and methanol (3:1)-water with 0.5% (v/v) formic acid.

Equilibrium solubility values were determined by slurring the excess amount of the co-crystals in 1.5 mL of pH pH = 2.0 Na_2HPO_4-H_3PO_4 buffer at room temperature for 24 h. The suspension was filtered through a 0.45 μm syringe filter, and the concentration of the resultant solution was determined. Intrinsic dissolution experiments were carried out on a PION uDISS apparatus using deionized water as dissolution medium. For IDR measurements, 8 mg of HCT and co-crystals **1**−**4** were placed in the dissolution attachments and compressed to a 0.07 cm^2 disc using a press at a pressure of 120 bar and hold for 3 min, respectively. The attachments were placed in 20 mL glass vessels prefilled with pH = 2.0 Na_2HPO_4-H_3PO_4 buffer at 37 ºC and rotated at 75 rpm. The solution was filtered through 0.45 μm syringe filter. The resulting filtrate was processed and the concentration was measured by HPLC. Confirmed by PXRD analysis, there is no form transformation observed upon compression and throughout the dissolution and solubility experiments.

Results and discussion

Reaction crystallization approach was found to be effective in preparation of HCT co-crystals. Excess amount of co-formers were pre-dissolved into ethyl acetate to give a saturated solution, followed by addition of HCT to allow the formation of the desired co-crystals. The HCT molecule possesses a considerable potential for intermolecular interactions with co-former molecules via three functional groups (the sulfonamide groups SO_2NH_2 and SO_2NH, and the NH group), which can give rise to hydrogen bonding with corresponding co-formers. The variety of hydrogen bonding interactions found in the co-crystals characterized in this work are depicted in Scheme 2 and discussed individually in the following sections separately.

Crystal Structure Analysis

Complex **1** is a 1:1 co-crystal of HCT and pyrazinamide as revealed by the single crystal structure. Crystal data and refinement parameters for co-crystal **1** are listed in Table 2. Crystals of compound **1** crystallized in the orthorhombic $P2_12_12_1$ space group. The asymmetric unit consists of one HCT molecule and a pyrazinamide molecule. As expected, H-bonding interactions are dominant in the crystal structure. The co-crystal structure can be interpreted as two sets of H-bonding network constructed by HCT and pyrazinamide molecules itself, respectively. The sulfonamide moieties of HCT form a H-bonding with adjacent amino group via N_2-$H_2\cdots O_3$=S interactions (2.26 Å) to form a 1D infinity chain structure along *b* axis (Figure 1a). On the other hand, homo 1D H-bonding chain structures are also observed in pyrazinamide molecules connected by amide moiety and pyridyl nitrogen in a head-to-tail fashion also along *b* axis (Figure 1b). The different 1D polymeric chains formed by HCT and pyrazinamide consequently intertwined and positioned perpendicular with each other (Figure 1c). Hetero molecular H-bonding was also observed between the carbonyl moiety of the amide group in pyrazinamide molecules and the sulfonamide moiety of HCT molecules (synthon **IV**, N_3−$H_4\cdots O_5$: 2.32 Å) to give a 2D sheet structure (Figure 1c). The overall supramolecular hydrogen bonding results in 3D architecture that are stabilized by offset π-π stacking[19] with centroid–centroid distance of 3.67Å as represented in Figure 1d. It is interesting that co-crystal **1** exhibits regular "honeycomb" pattern when viewed from the *a* axis (Figure 1d). Geometrical parameters for hydrogen bonds in co-crystals **1**−**4** were summarized in Table S1 (ESI†).

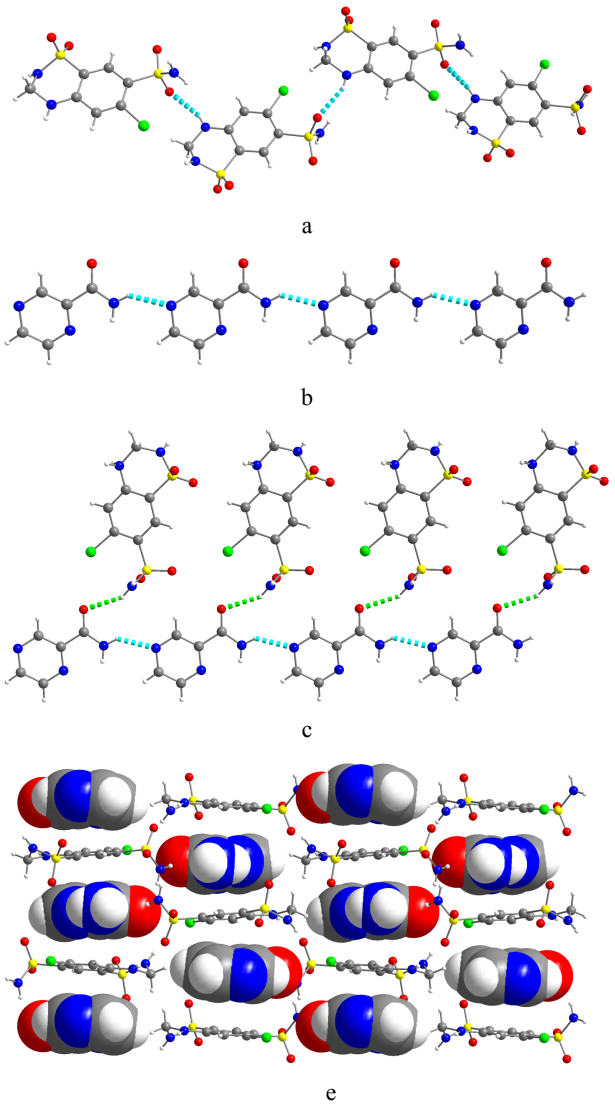

Figure 1. (a) The 1D HCT chain, (b) the 1D pyrazinamide chain, (c) 3D architecture and (e) pyrazinamide in spacefill model of **1**.

Co-crystallization of HCT with 4,4'-bipyridine in a EtOAc solution at ambient conditions afforded complex **2** as a hydrate. The crystal structure belongs to the monoclinic system in space group $P2_1/n$. The asymmetric unit consisting of two HCT, three 4,4'-bipyridine, and two water molecules (Figure 2a). H-bonding and π-π stacking are dominant interactions in the single crystal structure of **2**. Two HCT molecules and a bipyridine molecule packed in a "sandwich" fashion (Figure 2a), with the centroid-centroid distance of 3.93 Å between HCT and 4,4'-bipyridine. Then one "sandwich" unit interacts to another via synthon **I** N_3–H_3···N_6 (distance of 2.17 Å) and π-π stacking (centroid–centroid distance of 3.78 Å, Figure 2b) between bipyridine molecules as represented in Figure 2c to form infinite 1D polymeric chains. Interestingly, water molecules in **2** exist in a DDAA[15] environment that form tunnels parallel to *a* axis. Act as both H-bonding donor and acceptor, water molecules plays important roles in building the H-bonding network. Four distinctive H-bonding interactions are associated with each water molecule, including two H-bonding formed between water and pyridyl nitrogen via O_{1S}–H_{1S}···N_4 (2.00 Å), O_{1S}–H_{2S}···N_5 (2.03 Å) and another two H-bonding interactions build between water and sulfonamide moieties of HCT molecules via N_1–H_1···O_{1S} (1.96 Å) and N_3–H_4···O_{1S} (2.27 Å). It was through the multiple H-bonding interaction between water and the host molecules to connect the 1D "sandwich" chains to form a 2D structure in Figure 2d.

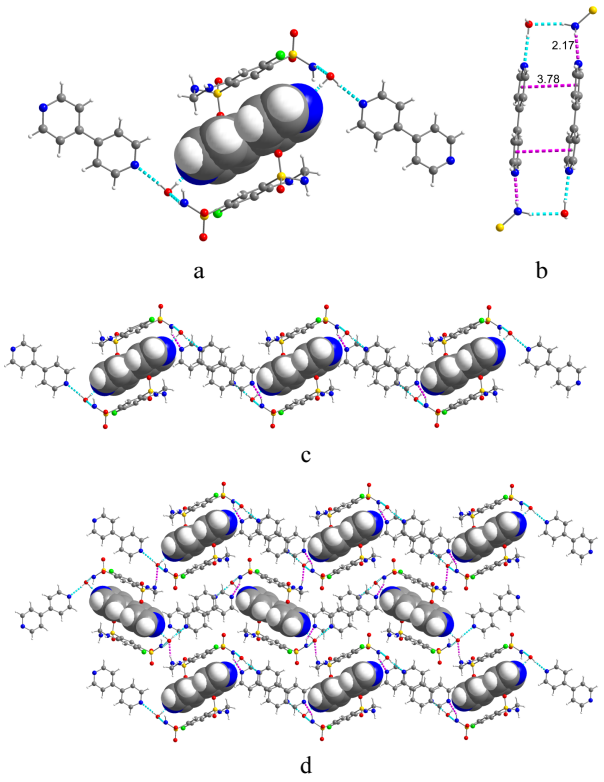

Figure 2. (a) The asymmetric unit, (b) π-π stacking, (c) 1D perpendicular chain, (d) 2D architecture of **2**.

HCT and 1,2-bis(4-pyridyl)ethane form a 1:1 co-crystal of **3** in monoclinic space group $P2_1/n$ with $Z = 4$. the asymmetric unit consists of a molecule of HCT and a molecule of 1,2-bis(4-pyridyl)ethane. A tetramer structure constructed by two HCT molecules and two bipyridyl molecules was identified in the structure (Figure 3a). Major H-bonding interactions involved synthon **I** N_1–H_1···N_5 (distance of 1.83 Å) and N_3–H_4···N_4 (distance of 2.15 Å). The cyclic tetramer was found to further extend into 2D V-shaped structures via N_2–H_2···N_2 (distance of 2.36 Å) interaction (Figure 3b).

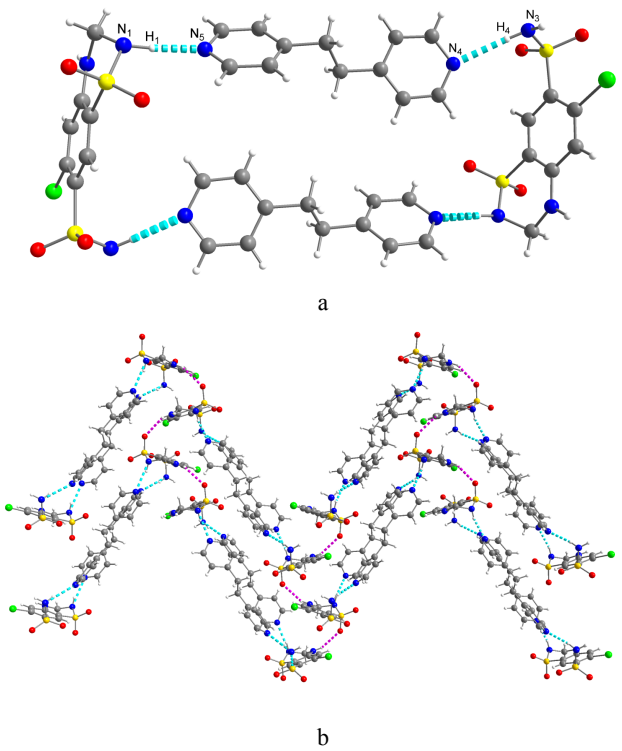

Figure 3. (a) The cyclic heterotetramer and (b) zigzag-shaped stacking of **3**.

The bipyridyl co-formers of **3** and **4** have very similar functionality and molecular geometry, however, the slight differences in the bridging ethylene moiety have alter the co-crystal structures significantly. Co-crystal of **4** crystallized in monoclinic $P2_1/n$ space group. Unlike the formation of tetramer structure in complex **3**, the crystal structure reveals that **4** contains two HCT and four *trans*-1,2-bis(4-pyridyl)ethylene molecules in the asymmetric unit. The bipyridyl molecules aligned in parallel with obvious offset. Intermolecular H-bonding interactions observed through synthon **I**, $N_1{-}H_1{\cdots}N_4$, $N_3{-}H_3{\cdots}N_5$, $N_3{-}H_4{\cdots}N_6$, $N_{1'}{-}H_{1'}{\cdots}N_7$, and $N_{3'}{-}H_{3'}{\cdots}N_8$ (distance of 2.39, 2.38, 2.10, 2.43, and 2.15 Å, respectively), to formation of a *Z*-shaped heterohexamer (Figure 4a). The *Z*-shaped heterohexamer further extended into a well defined 2D H-bonding network through weak =C-H hydrogen bonding [20] of $N_{37'}{-}H{\cdots}N_{7'}$ (distance of 2.81 Å) and $N_{35'}{-}H{\cdots}O_1$ (distance of 2.98 Å) as depicted in Figure 4b. No π-π stacking was observed throughout the crystal structure. Noticeably, the double bond distance between bipyridyl was determined as 4.30 Å.

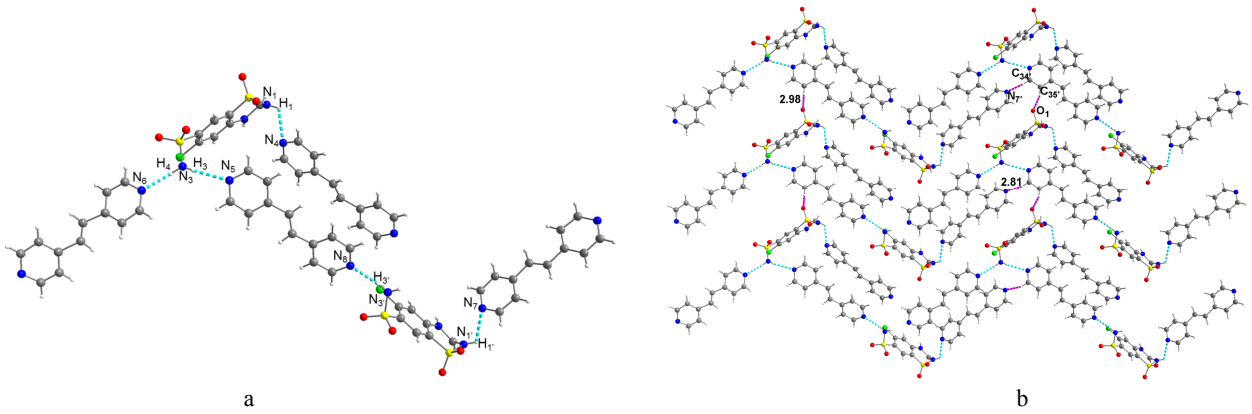

Figure 4. (a) *Z*-shaped heterohexamer and (b) zigzag-shaped stacking of **4**.

CrystEngComm RSCPublishing

ARTICLE

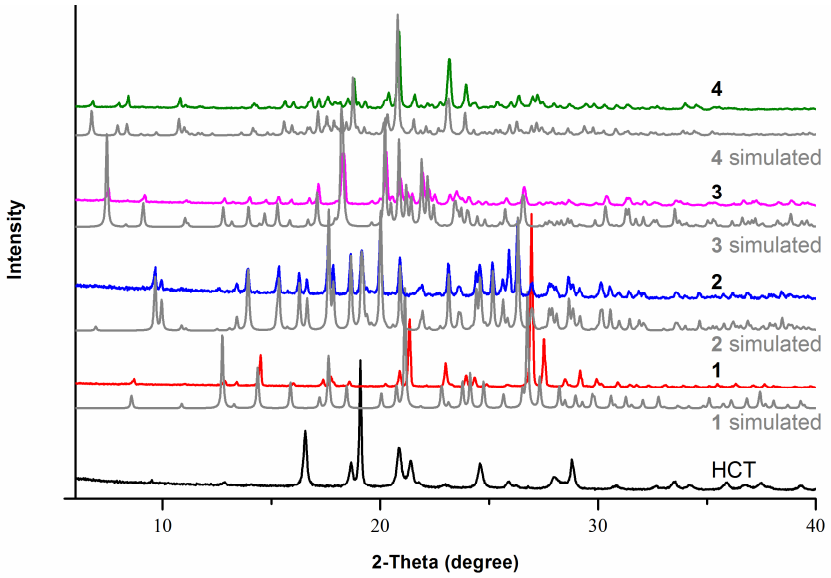

Figure 5. PXRD patterns of HCT and its co-crystals **1**–**4**.

Characterization and thermal properties

All the co-crystals **1**−**4** were thoroughly characterized by powder X-ray diffraction, FT-IR, Raman, and thermal analysis. The PXRD was used to check the phase purity of **1**−**4** (Figure 5). The results showed that the patterns of the products are different from either that of HCT or corresponding co-formers (Figure S1−S4, ESI†). In addition, all the peaks displayed in the measured patterns from bulk powder are closely matched with those in the simulated patterns generated from single crystal diffraction data, confirming the formation of the corresponding molecular complexes **1**−**4** in high phase purity. The thermal behaviors of HCT and **1**−**4** were investigated by DSC (Figure S5−S8, ESI†) and TGA (Figure S9, ESI†). It can be found that the melting points at 195.2, 138.1, and 168.2 °C for **1**, **3**, and **4**, respectively. The melting temperature of co-crystals are significantly different from those of HCT and corresponding co-formers. It is interesting to note that the melting temperature for **1**, **3**, and **4** is always found to be in-between those of HCT and corresponding co-formers, while the melting point for **2** is not observed. This can be attributed to the fact that **2** is crystallized as an unstable hydrate form, when the molecules of H_2O released from the crystal lattice at T_{onset} = 81.3 °C, the resulted material decomposed at T = 170.1 °C as the temperature further ramped up.

Solubility and dissolution study

Solubility and dissolution rate are important physico-chemical parameters for the estimation of bioavailability of pharmaceutical solids. Solubility is defined as the concentration of a pharmaceutical solid at the equilibrium between the solution and the undissolved solid, and the dissolution rate is defined as the rate at which this equilibrium state is reached. Solubility is a thermodynamic parameter. In this paper, we studied the solubility of the present three co-crystals by using Dissolution rate is a key parameter to be considered during the course of oral dosage form development. Since a drug has to be dissolved before it can be absorbed, the dissolution profiles could have profound influence on the pharmacokinetics and pharmacodynamics properties.[18b, c] For a better understanding of how the solid-state forms affect the dissolution behaviors, intrinsic dissolution rates and equilibrium solubility values of HCT and co-crystals **1**−**4** were investigated. The solubility of pyrazinamide, 4,4'-bipyridine, 1,2-bis(4-pyridyl)ethane, and *trans*-1,2-bis(4-pyridyl)ethylene were found to be 25, 9, 19, and 12 mg/mL, respectively (Table S2, ESI†). The equilibrium solubility of the HCT and co-crystals **1**−**4** were measured to be 0.55, 0.79, 0.63, 0.72, and 0.64 mg/mL, respectively (Table S2, ESI†). As depicted in Figure 6, HCT and **1**−**4** present different intrinsic dissolution rates of 47, 68, 52, 57, and 53 $\mu g/cm^2/min$, respectively. The co-crystal **1** has both improved solubility and IDR as 1.4 times as that of HCT itself. No phase transformation (monitored by PXRD and Raman) was observed after the IDR experiment.

Both solubility and IDR are following the same descending trend of **1** > **3** > **4** > **2** > HCT. This trend may be explained by the co-formers solubility rule: co-crystal solubility is directly proportional to the solubility of co-former, which means the more soluble co-formers leading to more soluble co-crystals.[21]

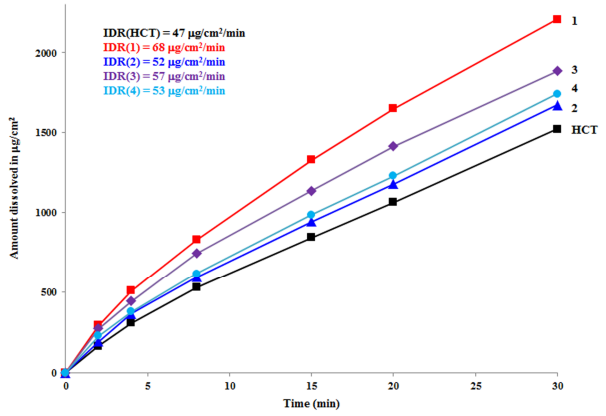

Figure 6. Intrinsic dissolution profiles of HCT and its co-crystals **1**–**4** in pH 2.0 phosphate buffer.

Conclusions

Pharmaceutical co-crystals represent an alternative approach to alter the physicochemical properties of APIs. The knowledge on this fascinating field has been recently widened because pharmaceutical co-crystals could be rational designed from a crystal engineering perspective. In this work, analysis of structural data in the Cambridge Structural Database resulted in the identification of a range of potential co-crystal formers compatible with HCT. Subsequent screening using reaction co-crystallization method in conjunction with high-throughput PXRD led to the discovery of four new co-crystals of HCT. Three different bipyridyl compounds were employed to form a set of co-crystal with HCT, the slight differences in the molecular structures of co-former have led to a drastic changes in H-bonding interactions and crystal packing. H-bonding formation between sulfonamide amino group and pyridyl moiety as synthon **I** is in a predictable interactions observed in co-crystals of **2**–**4**.

The HCT co-crystals reported in this work represent unique solid modifications and display obviously different physical and chemical properties comparing with their parent compounds. Particularly, the drug-drug co-crystal **1** is a promising candidate for improving the solubility and dissolution rate of HCT. Further studies should be conducted to see if drug-drug co-crystal **1** improve their bioavailability as potential solids for the delivery of combination drugs.

Acknowledgements

We thank the National Natural Science Foundation of China (Grant 81273479), Grants from Shanghai Institute of Materia Medica New-Star Plan B, and the Chinese Academy of Sciences for funding.

Notes and references

Pharmaceutical Analytical & Solid-State Chemistry Research Center, Shanghai Institute of Materia Medica, Chinese Academy of Sciences, Shanghai 201203, China

† Electronic supplementary information (ESI) available. Characterization data and CCDC 989055-989058. For ESI and crystallographic data in CIF or other electronic format see DOI:

‡ These authors contributed equally to the work.

1 J. W. Steed, *Trends Pharmacol. Sci.*, 2013, **34**, 185-193.
2 a) J.-R. Wang, C. Zhou, X. Yu and X. Mei, *Chem. Commun.*, 2014, **50**, 855-858; b) S. L. Morissette, Ö. Almarsson, M. L. Peterson, J. F. Remenar, M. J. Read, A. V. Lemmo, S. Ellis, M. J. Cima and C. R. Gardner, *Adv. Drug Deliver. Rev.*, 2004, **56**, 275-300; c) J. W. Steed, *Trends Pharmacol. Sci.*, 2013, **34**, 185-193; d) D. Good, C. Miranda and N. Rodriguez-Hornedo, *CrystEngComm*, 2011, **13**, 1181-1189; e) N. Huang and N. Rodriguez-Hornedo, *CrystEngComm*, 2011, **13**, 5409-5422; f) J. A. Perman, A. J. Cairns, L. Wojtas, M. Eddaoudi and M. J. Zaworotko, *CrystEngComm*, 2011, **13**, 3130-3133.
3 S. M. Berge, L. D. Bighley and D. C. Monkhouse, *J. Pharm. Sci.*, 1977, **66**, 1-19.
4 R. K. Khankari and D. J. Grant, *Thermochim. Acta*, 1995, **248**, 61-79.
5 S. R. Vippagunta, H. G. Brittain and D. J. Grant, *Adv. drug delivery rev.*, 2001, **48**, 3-26.
6 a) Z. R. Ranjbar, A. Morsali and L.-G. Zhu, *J. mol. struct.*, 2007, **826**, 29-35; b) S. P. Velaga, S. Basavoju and D. Boström, *J. mol. struct.*, 2008, **889**, 150-153; c) N. Ravikumar, G. Gaddamanugu and K. Anand Solomon, *J. mol. struct.*, 2013, **1033**, 272-279; d) M. Sowa, K. Ślepokura and E. Matczak-Jon, *J. mol. struct.*, 2014, **1058**, 114-121.
7 O. Almarsson and M. J. Zaworotko, *Chem. Commun.* , 2004, 1889-1896.
8 a) Y. Yan, J.-M. Chen, N. Geng and T.-B. Lu, *Cryst. Growth Des.*, 2012, **12**, 2226-2233; b) G. R. Desiraju, *Angew. Chem. Int. Ed.*, 1995, **34**, 2311-2327; c) P. A. Wood, N. Feeder, M. Furlow, P. Galek, C. R. Groom and E. Pidcock, *CrystEngComm*, 2014; d) D. Berry, S. Coles and N. Blagden, *CrystEngComm*, 2014.
9 C. B. Aakeroy and D. J. Salmon, *CrystEngComm*, 2005, **7**, 439-448.
10 C. F. Macrae, I. J. Bruno, J. A. Chisholm, P. R. Edgington, P. McCabe, E. Pidcock, L. Rodriguez-Monge, R. Taylor, J. v. Streek and P. A. Wood, *J. Appl. Crystallogr.*, 2008, **41**, 466-470.
11 I. J. Bruno, J. C. Cole, P. R. Edgington, M. Kessler, C. F. Macrae, P. McCabe, J. Pearson and R. Taylor, *Acta crystallogr. B*, 2002, **58**, 389-397.
12 R. Chadha, S. Bhandari, D. Kataria, S. Gupta and D. Singh Jain, *J. Microencapsul.*, 2012, **29**, 805-812.
13 S. Padmapriya, N. Rajendran and V. Ravichandiran, *Int. J. PharmTech Res*, 2011, **3**, 1509-1514.
14 A. M. L. Denadai, M. M. Santoro, L. H. D. Silva, A. T. Viana, R. A. S. Santos and R. D. Sinisterra, *J. Incl. Phenom. Macro.*, 2006, **55**, 41-49.
15 H. D. Clarke, K. K. Arora, H. Bass, P. Kavuru, T. T. Ong, T. Pujari, L. Wojtas and M. J. Zaworotko, *Cryst. Growth Des.*, 2010, **10**, 2152-2167.
16 P. Sanphui and L. Rajput, *Acta crystallogr. B*, 2014, **70**, 81.
17 a) S. Aitipamula, P. S. Chow and R. B. Tan, *CrystEngComm*, 2009, **11**, 1823-1827; b) A. Delori, P. T. A. Galek, E. Pidcock, M. Patni and W. Jones, *CrystEngComm*, 2013, **15**, 2916-2928.
18 a) T. Lee and F. B. Hsu, *Drug Dev. Ind. Pharm.*, 2007, **33**, 1273-1284; b) T. Lee and G. D. Chang, *Cryst. Growth Des.*, 2009, **9**, 3551-3561; c) T. Lee and C. W. Zhang, *Pharm. Res.*, 2008, **25**, 1563-1571.
19 C. Janiak, *J. Chem. Soc., Dalton Trans.*, 2000, 3885-3896.
20 G. R. Desiraju, *Acc. Chem. Res.*, 1996, **29**, 441-449.
21 a) D. J. Good and N. r. Rodríguez-Hornedo, *Cryst. Growth Des.*, 2009, **9**, 2252-2264; b) D. J. Good and N. Rodríguez-Hornedo, *Cryst. Growth Des.*, 2010, **10**, 1028-1032.

Structural and physicochemical aspects of hydrochlorothiazide co-crystals

Jian-Rong Wang, Chanjuan Ye, and Xuefeng Mei*

Pharmaceutical Analytical & Solid-State Chemistry Research Center, Shanghai Institute of Materia Medica, Chinese Academy of Sciences, Shanghai 201203, China.

E-mail: jrwang@ simm.ac.cn, chanjuanye@ simm.ac.cn, xuefengmei@simm.ac.cn.

SYNOPSIS: The drug-drug co-crystal of hydrochlorothiazide with pyrazinamide is a potential candidate for development of hydrochlorothiazide formulations for combinational therapy.

TOC: